Atmospheric plasma spraying of functionally graded steel/tungsten layers for the first wall of future fusion reactors

S. Heuer[a,*], J. Matějíček[b], M. Vilémová[b], M. Koller[c], K. Illkova[b], J. Veverka[b], Th. Weber[a], G. Pintsuk[a], J.W. Coenen[a], Ch. Linsmeier[a]

[a] *Forschungszentrum Jülich GmbH, Institut für Energie- und Klimaforschung - Plasmaphysik, Partner of the Trilateral Euregio Cluster (TEC), 52425 Jülich, Germany*
[b] *Institute of Plasma Physics, Czech Academy of Sciences, 182 00 Praha 8, Czech Republic*
[c] *Institute of Thermomechanics, Czech Academy of Sciences, 182 00 Praha 8, Czech Republic*

Abstract

Functionally graded steel/tungsten layers may be used as interlayers in the first wall of future fusion reactors to balance thermally-induced stress peaks in the steel-tungsten joint. In this work, a modified water-stabilized atmospheric plasma spraying set-up is used to deposit uniform and functionally graded steel/tungsten coatings at elevated substrate temperatures. Uniform coatings were used to characterise individual sublayers of graded coatings in detail. The thermal expansion, thermal conductivity, Young's modulus and yield strength of the layers are promising for the application in steel-tungsten joints and can be explained by microstructural observations. Only at a substrate preheating temperature of 900°C the formation of intermetallic precipitates during deposition was observed.

Keywords:
Atmospheric Plasma Spraying (APS), Functionally Graded Materials (FGM), tungsten-steel composite materials, nuclear fusion, DEMO, first wall

1. Introduction

In a fusion reactor, plasma facing components (PFC) encompass the hot plasma. Materials relevant for PFC have to tolerate severe thermal, physical and mechanical loads. With respect to the future demonstration power plant, DEMO, tungsten (W) is considered the prime plasma facing material used in the first wall of PFC [1, 2]. Several design studies suggest to join a thin layer (2-3 mm) of this material to a structure made of Eurofer steel [3–5]. Resulting from discretely changing material properties at this dissimilar materials joint, high thermally-induced macro stresses develop during production and in operation, which may yield premature failure of the first wall [6]. The following aspects have to be considered for joining W and steel, in consequence, particularly when focussing on fusion applications.

1. the coefficients of thermal expansion (CTE) of Eurofer and W differ strongly (12.0 x 10^{-6} K^{-1} vs. 4.4 x 10^{-6} K^{-1} at room temperature), causing high macro stresses in the joint [6–9]
2. the pulsed operation of DEMO creates cyclic heat loads in the first wall, which may induce fatigue damage in the joint when no stress-relieving interlayers are implemented [10]
3. high reactor heat loads may cause temperatures above the tolerable temperature window of commonly used interlayer materials (e.g. Cu brazes) [6, 10, 11]
4. the presence of neutrons in the fusion environment prohibits the utilisation of some commonly used interlayer materials (e.g. Ag brazes, Ni) due to the formation of long-living nuclides [12]
5. the solidus temperatures of Eurofer and W differ strongly (1550°C vs. 3400°C) [7–9]
6. intermetallic Fe_xW_y precipitates form during extended high temperature exposure [13]

For the named reasons, the fabrication of the first wall of DEMO requires tailored joining techniques. A potential route is to implement a graded steel/W interlayer between the Eurofer structure and the W armour. So-called functionally graded steel/W materials (steel/W FGMs) exhibit a smooth material transition from the W-rich end to the steel-rich end across the interlayer's height, macroscopically. In a joint, this helps redistributing thermally-induced macro stress peaks and, eventually, may prevent fatigue damage [6, 10, 11]. When applied directly on the bulk W armour, the steel-rich end of the FGM can be joined to the Eurofer structure by diffusion bonding at fairly low temperatures [14]. The procedure already tackles aspects 1 to 4 of the aforementioned list of required considerations for joining steel and W. To tackle aspects 5 and 6 of the list, several studies were carried out, trying to identify feasible processing techniques for steel/W FGM fabrication. Among the techniques are atmospheric plasma spraying (APS) [15, 16], laser cladding

*Corresponding author
Email address: s.heuer@fz-juelich.de (S. Heuer)

[15], uniaxial hot pressing [15], spark plasma sintering (SPS) [15], vacuum plasma spraying (VPS) [16–19], physical vapor deposition (PVD) [19], electro-chemical deposition [20, 21], hot explosion pressing [19], and other field assisted sintering techniques (FAST) than SPS [22, 23]. While all named possibilities have shown technical feasibility at an early stage of research, plasma spraying and FAST are most promising so far. In general, APS is accompanied by higher oxide amount in the FGM compared to VPS and FAST, but it is advantageous in terms of technical simplicity. Larger areas may be covered compared to FAST and a less complex set-up is required compared to VPS.

In a previous study, pure W and pure steel layers were deposited using a modified APS set-up, referred to as water-stabilized plasma spraying, WSP (Institute of Plasma Physics, Czech Republic) [24]. The WSP set-up is equipped with an inert gas-filled shrouding chamber surrounding the substrate, as described in detail in [24]. Using an older version of the set-up that did not feature a shrouding chamber, mixed steel/W coatings were deposited [25]. Complementary to the previous studies, the current contribution explores the deposition of mixed steel/W coatings and FGMs using the described set-up. Since elevated preheating temperatures of the substrates up to 500°C have shown a positive impact on the thermal conductivity of sprayed layers [24], the preheating temperature is increased to 700°C and 900°C in the current contribution. Deposited coatings are characterised microstructurally, thermo-physically and mechanically.

2. Experimental

2.1. Layer deposition

The basic principle of plasma spraying consists in feeding powder particles into an expanding plasma stream that heats the particles and accelerates them towards a substrate. Moving the substrate and plasma stream in an array relatively to one another, the particles solidify on the substrate and create layers of constant thickness. The fast deposition and cooling may allow to limit production-introduced intermetallic precipitates in the steel/W material system. Following promising results of earlier work, the water-stabilized plasma torch described in [24] was used in the present study.

Two types of coatings were deposited on sand-blasted steel substrates (25 x 70 x 2 mm^3). Firstly, uniform steel/W coatings, each with a constant steel/W ratio, were produced. The nominal W volume fractions of these coatings were 0, 25, 50, 75 and 100 %. Secondly, actual FGMs were deposited by successively depositing steel/W layers of the named W volume fractions. Both uniform and graded coatings were approximately 25 x 60 x 2 mm^3 in size. An area of 10 mm width of the substrate remained mostly uncovered and was used for mounting the substrate to a holder.

For the deposition of tungsten, a 5:1 weight mixture of W (63–80 μm, Alldyne Powder Technologies, USA) and WC (40–80 μm, Osram, Czech Republic) powders was used. The WC powder was added to suppress in-flight oxidation through a reducing effect of carbon. For the deposition of steel, AISI410 (90–140 μm, Flame Spray Technologies, Netherlands) powder was used. Amounts of major alloying elements and of oxygen in the raw powders, measured by inductively coupled plasma emission spectroscopy (ICP-OES) and helium carrier gas hot extraction, are given in table 1. The powders were fed to the plasma stream via individual feeders.

Table 1: Compositions of sprayed raw powders as measured by ICP-OES and helium carrier gas hot extraction.

Powder	Element amount (wt.%)					
	W	Fe	Cr	C	O	other
W+WC (5:1)	96.3	0.03	0	0.72	0.016	bal.
410 steel	0	83.63	11.99	0.005	0.034	bal.

Both the carrier gas of plasma spraying and the shrouding gas were Ar + 7 vol.% H_2. Other spraying parameters (feed rates, spraying distance (SD) and feeding distances (FD)) are listed in table 2. While the feeding distances of W and steel were kept constant in all experiments, the spraying distance was varied between the optimum SD of W spraying and the optimum of steel spraying following the nominal volumetric steel/W ratio of the sprayed layer.

Preheating of the substrates to 500, 700 and 900°C was realised by focussing the plasma plume on the substrate prior to the actual deposition. Based on previous experience, the substrate temperature was maintained close to the preheating temperature during deposition by controlling the frequency of the torch passes and the shrouding gas flow rate [24]. The temperature was measured by a thermocouple attached to the area of the steel substrate that remained uncovered. Exploratory temperature measurements, using multiple thermocouples attached to the front side, back side and short edge of the substrate, allowed to take geometric temperature discrepancies across the substrate into account during spraying. As the temperature rose above the preheating temperature during spraying, after each five to ten spraying passes, the sample was allowed to cool down to the temperature of preheating. The maximum substrate temperature during spraying was 600–650°C for samples with preheating temperature of 500°C, 780–820°C for samples with preheating temperature of 700°C and 950-980°C for samples with preheating temperature of 900°C. For all subsequent analyses of the deposited layers, the steel substrates were removed.

2.2. Microstructural and elemental characterisation

For microstructural characterisation an EVO MA15 scanning electron microscope (SEM, Carl Zeiss SMT, Germany) was used. Porosity measurements and the quantification of actual volumetric steel/W compositions of deposited layers were carried out by quantitative image analysis of secondary electron contrast images of cross sections. For qualitative element analysis, energy dispersive spectroscopy (EDS) with a XFlash 5010 SDD detector (Bruker, Germany) was used. Oxygen amounts were measured by helium carrier gas hot extraction in a TCH 600 instrument (Leco, Germany).

Table 2: Processing parameters applied for the spraying of 410 steel/W coatings.

Material	Nominal W content (vol.%)	Preheating temperature (°C)	Spraying distance (mm)	Feeding distance W (mm)	Feeding distance 410 steel (mm)	Feed rate W ($Kg\,h^{-1}$)	Feed rate 410 steel ($Kg\,h^{-1}$)
0W	0	700	330	-	105	0	13.7
25W	25	700	300	30	105	10.5	8.7
50W	50	700	260	30	105	18	5
75W	75	700	230	30	105	24	2.2
100W	100	700	200	30	-	30	0
50W	50	500	260	30	105	18	5
50W	50	900	260	30	105	18	5

2.3. Thermo-physical characterisation

From the thermo-physical properties, the thermal conductivity at various temperatures (λ(T)) and the coefficient of thermal expansion (CTE) of the deposited uniform coatings were examined. The thermal conductivity was calculated according to equation (1), in which ρ represents the sample density, $\alpha(T)$ the thermal diffusivity and $c_p(T)$ the heat capacity.

$$\lambda(\mathrm{T}) = \rho\ \alpha(T)\ c_p(T) \tag{1}$$

The sample density was calculated from quantitative image analysis results, hence averages the densities of pure W, pure steel, and pores according to their share in the images. Temperature dependence of the density was not considered for the calculation of heat conductivity as its impact is of minor relevance.

Thermal diffusivity and heat capacity were measured by the laser flash method at room temperature, 200, 400, 600 and 800°C, using an LFA 1000 instrument (Linseis, Germany). Two pieces of free-standing coatings with ca. 2 mm thickness were used. The measurements were carried out in vacuum; five measurements were taken at each temperature.

The CTE was calculated from thermal elongation experiments using a LV75 dilatometer (Linseis, Germany). Due to limited material availability, small rectangular non-standard samples (5 x 4 x 2 mm^3) were extracted, ground and placed between two 10 mm long alumina rods. The set-up achieves standard sample length of 25 mm and uses the temperature sensitivity of the dilatometer to full capacity. Prior to actual measurements, the set-up accuracy was verified using small and regular scale pure W rods. Heating rate and maximum testing temperature of the dilatometer were set to 3 $K\,min^{-1}$ and 1060°C. The latter was kept for 15 min before the furnace was allowed to cool down to room temperature.

2.4. Mechanical characterisation

With respect to mechanical characterisation, Young's modulus, yield strength and ultimate bending strength were examined. For the measurements, the limited amount of available material and the challenging machinability of W had to be considered.

Room temperature elastic properties of uniform coatings were measured by resonant ultrasound spectroscopy (RUS) [26, 27]. From the coatings, rectangular parallelepiped samples with dimensions of a few millimetres were cut, having one of the principal directions parallel to the spraying axis. First, velocities of longitudinal waves along the principal directions were measured by pulse-echo method in order to confirm elastic anisotropy of the coatings. Due to the microstructure, the coatings exhibit transverse isotropic symmetry with 5 independent elastic coefficients. Resonant spectra of free vibrations were measured at 20°C by laser-based contactless RUS, where the vibrations of a sample are generated by pulses of an infrared laser beam, and detected by a scanning laser vibrometer on one side of the sample. The elastic coefficients are determined inversely, where a resonant spectrum is calculated from the given set of elastic coefficients, sample density (mentioned above) and dimensions, and it is iteratively compared with the measured resonant spectrum until the sum of squared differences between the calculated and measured resonant frequencies is minimized. From the set of elastic coefficients determined by RUS, Young's moduli in the principal directions of the coatings are obtained.

Measurement of yield strength and ultimate strength was carried out via a modified four-point bending method, following bending tests of powder-injection-moulded W samples [28]. For sample preparation, small bars of quadratic cross section (12 x 1 x 1 mm^3) were extracted from the uniform coatings by electric discharge machining (EDM). The orientation of the bars before extraction was marked in order to later mimic stresses of the reactor operation by applying bending stresses in the deposition plane. All four longitudinal surfaces were ground and polished to mirror finish (0.25 μm colloidal silica) to remove EDM cracks and roughness. Particular attention was paid to maintain planar surfaces during grinding and polishing. For testing, the lower supports were set 10 mm apart, the upper load distance was 5 mm and the vertical displacement speed 0.033 $mm\,s^{-1}$.

Exploratory four-point bending tests with steel/W samples following the procedure described in [28] sometimes yielded fracture outside the inner supports. Hence, bending stresses were inaccessible. In consequence, a notch, 0.1 mm wide and 0.15 mm deep, was introduced in the middle of the bottom side of the polished samples by EDM, assuring fracture at this position. The stress exaggeration factor of this notch was calculated by both finite element analysis (FEA) and by comparing test results of pure W bars cut from bulk material with and without notch, respectively. While the FEA yields an exaggeration fac-

tor of 2.8, the comparison of notched and un-notched pure W samples results in a factor of 2.1. Taking the mean stress exaggeration factor, 2.5, of the two independent evaluation methods and the standard test method of macroscopic four-point bending, ASTMD7264 [29], into account, bending stresses σ_b can be calculated by eq. (2). Here, F_b equals the load, d_{sup} the support distance, w the sample width and h the sample height.

$$\sigma_b = 2.5 \frac{3\, F_b d_{sup}}{4wh^2} \quad (2)$$

Bending experiments were carried out at 20 and 300°C in air using a universal testing machine (Zwick/Roell, Germany).

3. Results and discussion

3.1. Microstructural characterisation

Exemplary overview cross sections of uniform coatings and a steel/W FGM, all deposited on substrates that were preheated to 700°C, are shown in fig. 1. The microstructures of the FGM are similar to the uniform coatings, suggesting that the characterisation of uniform layers helps to understand properties of the individual sublayers of the FGM. Layered structures can be observed in the micrographs, which result from the impact and solidification of molten metal droplets during spraying. Four constituents are distinguishable from one another and are indicated in the images. Besides layered steel and W splats, layered oxides and irregularly shaped pores are present between the splats. Overview cross sections of layers deposited on substrates preheated to 500 and 900°C exhibit no other visible microstructural features than the ones presented in fig. 1, and hence are not shown here. X-ray diffractograms of coatings containing 25 to 75 vol.% W, deposited at 700°C, are shown in fig. 2 and confirm the observed phases. Particularly, no WC from the W+WC powder is indicated as WC is reduced to pure W during spraying.

Quantitative compositions of the layers are slightly different from the target compositions and are listed in tab. 3. With plasma spraying, several factors have an effect on the deposition efficiency, among them the spraying distance and the substrate temperature [32]. Both of these parameters were varied in the current experiments (cf. tab. 2), which may explain the discrepancies to nominal compositions. Apart from that, the presence of pores reduces the actual steel and W content. The porosity of all coatings varies between 1.9 and 5.5 vol.%. Despite the measured differences, no correlation between porosity and composition, or porosity and preheating temperature can be identified. Compared to previous work [24], in which pure W and pure 410 steel coatings were deposited at similar conditions to this work, the porosity of coatings presented here is about 2 vol.% higher. For the mixed steel/W layers, the elevated porosity may be explained by the spraying distance, which was set between the optimum distance for spraying W and steel according to the nominal steel/W ratio of each layer. Hence, neither pure W droplets, nor pure steel droplets experienced ideal spraying temperatures and velocities. Given somewhat lower porosities

Table 3: Measured thermo-physical and mechanical properties of deposited coatings and the reference materials tungsten, 410 steel, and Eurofer. * not measured, ** sample failed before measurement.

Material	Nominal W content (vol.%)	Preheating temperature (°C)	W content (vol.%)	Steel content (vol.%)	Porosity (vol.%)	Oxygen (wt.%)	Oxygen (at.%)	CTE 20-400 °C (10^{-6} K^{-1})	CTE 200-800°C (10^{-6} K^{-1})	Thermal conductivity at 400°C (W m^{-1} K^{-1})	Thermal conductivity at 800°C (W m^{-1} K^{-1})	Young's modulus E1 (GPa)	Young's modulus E3 (GPa)	E1/E3	Yield strength at 20°C (MPa)	Yield strength at 300°C (MPa)	Ultimate strength at 20°C (MPa)	Ultimate strength at 300°C (MPa)
0W	0	700	0	97	3	2	6.64	12.8	14.0	23.4	24.9	191.4	185.5	1.03	813	665	863	757
25W	25	700	22.1	72.4	5.5	0.84	3.98	12.3	11.0	25.8	28.8	179.9	160.1	1.12	688	838	756	788
50W	50	700	43.3	54.3	2.4	0.69	4.27	10.7	9.4	31.8	35.7	198.3	170.8	1.16	1335	982	1400	1178
75W	75	700	65.4	32.6	2	0.2	1.61	6.3	6.8	40.0	43.3	241.1	188	1.28	**	**	**	**
100W	100	700	96	0	4	0.027	0.3	7.5	7.4	66.2	61.4	229.1	193.4	1.18	557	731	629	894
50W	50	500	51.5	46.6	1.9	0.224	1.55	*	*	*	*	*	*		*	*	*	*
50W	50	900	42.8	54	3.2	0.57	3.52	*	*	*	*	*	*		*	*	*	*
bulk W [7]			100	0	0			4.4		138	120	397			1360	1050	1360	1070
bulk 410 steel [30, 31]			0	100	0			12.0		28		215			> 450	> 365	> 650	
bulk Eurofer [8, 9]			0	100	0			12.3		28	29.7	217			546	467	660	550

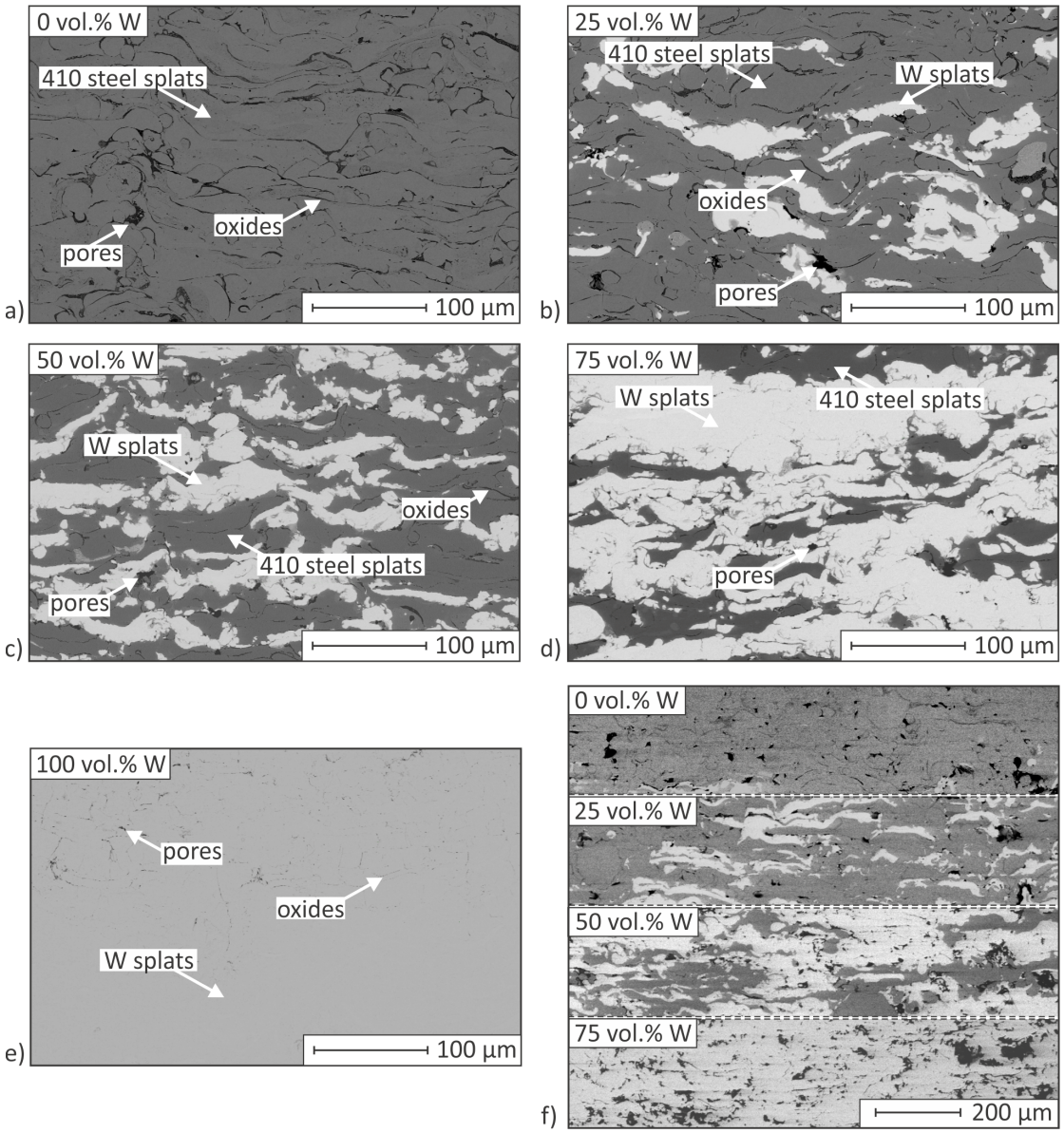

Figure 1: Cross sections of layers, deposited on substrates that were preheated to 700°C. a) 0 vol.% W, b) 25 vol.% W, c) 50 vol.% W, d) 75 vol.% W, e) 100 vol.% W f) FGM.

of mixed steel/W layers in [25], in which no shrouding chamber was used, but the spraying distance was kept constant (300 mm) close to the ideal steel spraying distance, the porosity of steel/W layers seems to be most sensitive to deviations from the ideal steel spraying distance. In the micrographs of fig. 1, the majority of pores is either located within pure steel volumes or at steel-W boundaries, supporting this impression. An explanation for the high porosity of pure coatings remains open.

Other than the porosity, the oxygen content decreases gradually from 6.6 to 0.3 at.% with increasing W content. A comparison of the oxygen content of the pure layers to the content of the used raw powders (410 steel: 0.12 at.% O, W+WC: 0.19 at.% O) indicates that mainly steel oxidises during spraying. Element maps based on EDS, shown in fig. 3, confirm this result, indicating that oxide volumes mainly contain O, Fe and Cr. The inverse correlation of oxygen and W content is caused by several effects. First, parts of the stronger oxidising steel are replaced by less sensitive W. Secondly, only the W powder was mixed with WC powder, following that an increasing W content is accompanied by stronger oxide-reducing capabilities. Lastly, the shorter spraying distances, which were used here with higher W contents, cause less interaction of molten droplets with oxygen in the flight phase of spraying. Regarding the last-mentioned effect, in [24] a decrease of oxygen by > 1 wt.% (ca. 10 at.%) was documented upon reducing the spraying distance of W+WC from 300 to 200 mm while other parameters were kept largely constant. A similar behaviour is assumed here for steel coatings and mixed coatings. In general, the positive impact of a shorter spraying distance on the oxidation of mixed steel/W layers, and its negative impact on the porosity

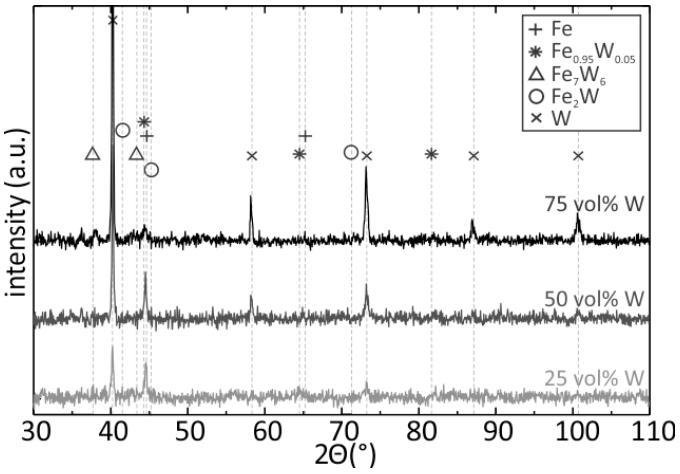

Figure 2: Representative X-ray diffractograms of coatings nominally containing 25, 50 and 75 vol.% W, deposited on substrates that were preheated 700°C.

resulting from the sensitivity of steel have to be balanced. An adjustment of the spraying distance is always necessary with respect to the specific application of the layers.

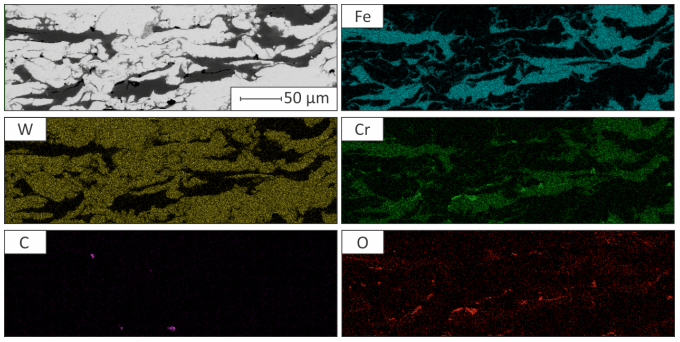

Figure 3: Representative element maps of coatings nominally containing 50 vol.% W, deposited on substrates that were preheated 700°C. The element distribution in this cross section was derived from EDS. Oxides contain O, Cr and Fe.

Besides the spraying distance, the substrate preheating temperature plays an important role for oxidation. While elevated preheating temperatures influence the coating cohesion positively [33], this may enhance oxidation. In the current work no obvious correlation between preheating temperature and oxygen amount was found for mixed steel/W layers (cf. tab. 3). In coatings nominally containing 50 vol.% W, deposited on 500, 700 and 900°C hot substrates, the oxygen amount varies between 1.55 and 4.27 at.%, and seems to be governed by slight variations of the steel/W ratio, rather than by the substrate temperature. This result correlates with observations in [24], in which no strong impact of the substrate preheating temperature on the oxidation of pure W and pure 410 steel layers was found. It also proves a positive impact of the shrouding chamber and suggests that oxides primarily form during the flight phase of the spraying process.

Given the limited oxidation of deposited material and the increased cohesion with elevated temperatures, high substrate preheating temperatures seem favourable for the deposition of steel/W coatings. However, the temperature-related precipitation of Fe_xW_y and $Fe_xCr_yW_z$ intermetallics has to be considered, too. In the micrographs of fig. 4, representative boundaries between steel and W volumes of steel/W layers with nominal 50 vol.% W deposited on different preheated substrates are shown. While steel and W volumes of layers deposited on substrates preheated to 500 and 700°C exhibit discrete interfaces, higher preheating temperatures cause accelerated interdiffusion. In consequence, coatings deposited on 900°C preheated substrates contain a solid solution seam and an intermetallics seam along the steel-W interface. Due to their brittleness and low thermal conductivity [34], intermetallics are undesired.

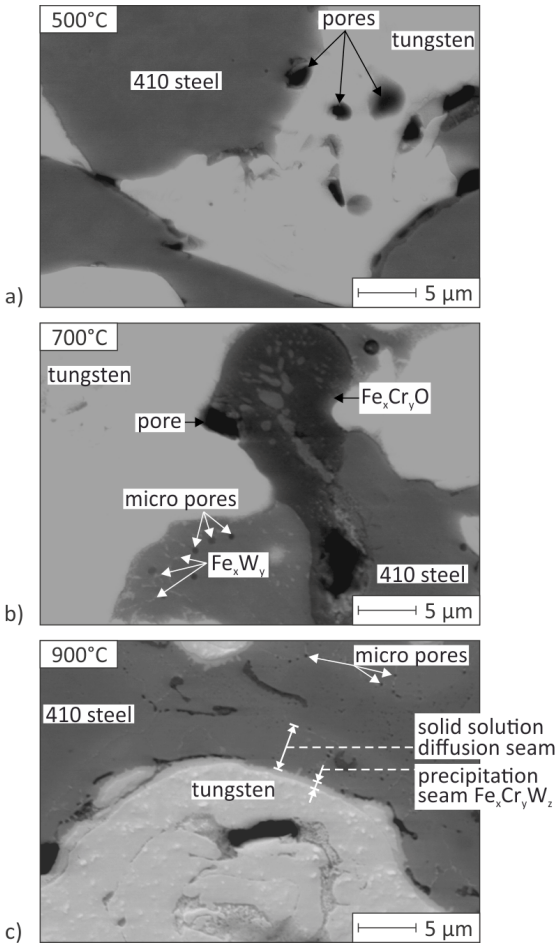

Figure 4: Representative boundary regions of individual W and steel volumes in coatings nominally containing 50 vol.% W, deposited on substrates that were preheated to a) 500°C, b) 700°C, and c) 900°C.

3.2. Thermo-physical characterisation

Relevant thermo-physical properties of the sprayed coatings with respect to the application in the first wall of fusion reactors are the CTE and the thermal conductivity. The CTE is important because the implementation of graded steel/W layers aims at levelling macro stress peaks at the W armour-Eurofer structure joint of the first wall by gradually converging the thermal expansion. The thermal conductivity is important because the

first wall has to ensure efficient heat removal from the fusion plasma. Both of the properties of steel/W coatings, deposited on 700°C preheated substrates, are listed in tab. 3 and shown in fig. 5.

Expansion coefficients are given with respect to two temperature ranges. The first set refers to a widely used temperature range in CTE reporting (20-400°C) and the second to a temperature range of interest for the current application (200-800°C). The results of both sets are similar. Comparing the measurement results with the CTE of pure bulk W and pure bulk steel, the realisation of gradual convergence via a graded layer is possible. While sprayed pure steel coatings show a similar CTE to bulk 410 steel and bulk Eurofer steel, sprayed pure W layers expand somewhat stronger than bulk W. Nevertheless, implementing graded mixed steel/W layers of the examined coatings in a steel-W joint may reduce the gap of CTE significantly. Apart from this result, the dilatometry measurements carried out to 1060°C have shown a complete reversal of temperature-induced expansion after cooling to room temperature. No residual expansion, e.g caused by excessive formation of intermetallics, was observed.

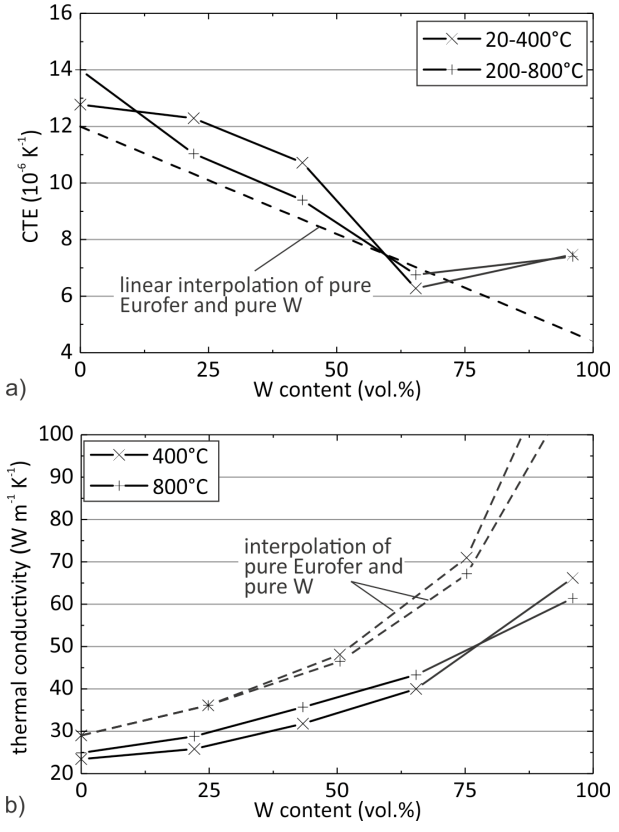

Figure 5: Thermo-physical properties of uniform coatings, deposited on substrates that were preheated to 700°C. a) Coefficient of thermal expansion, measured in two temperature windows, b) thermal conductivity, measured at two temperatures. The interpolation follows the parallel model [35].

The thermal conductivity of the coatings is presented in tab. 3 and fig. 5 b) at two temperatures, 400°C and 800°C. At 400°C, the thermal conductivity progressively increases with the W content in sprayed layers. Due to the presence of oxides and pores, sprayed pure 410 steel layers show 17 % lower thermal conductivity compared to 410 steel bulk material. Although less oxides were observed in W-rich coatings compared to steel-rich coatings, pure W coatings only reach approximately 50 % of the conductivity of bulk W. This paradox is because the thermal conductivity does not only depend on the amount of oxides itself, but rather on the quality of interfaces. While oxides at splat interfaces in the steel coatings are thicker than in W coatings, making the interfaces visually more prominent, steel splats (including Fe-Cr-oxides) do not necessarily reflect worse bonding compared to W splats. For the aimed application in the first wall, the measured conductivity is sufficiently high, but it indicates weak bonding of W splats enhancing the scattering of phonons. With elevated temperatures, the conductivity of coatings that contain steel increases slightly, whereas pure W layers show a reduced conductivity. These observations base on the strong increase of heat capacity of 410 steel with temperature, and the strong decrease of thermal diffusivity of W, respectively. They are in line with literature, which confirms the observations for pure steel and W [7, 30, 31]. After the high-temperature exposure, the thermal conductivity of the coatings was measured again and a slight increase was observed. For the pure steel, the increase was 6 %, for pure W it was 0.4 %; intermediate values were observed for the composites. This indicates that some sintering took place at the splat interfaces, expectedly to a higher extent in steel.

3.3. Mechanical characterisation

To guarantee structural integrity of the first wall, materials applied there have to provide satisfactory mechanical properties. In this work, the elastic modulus, the yield strength and the ultimate bending strength are assessed. The properties of pure and mixed steel/W coatings, deposited on 700°C preheated substrates, are listed in tab. 3 and shown in figs. 6 and 7.

With respect to Young's modulus, two values, E1 and E3, are given for each layer to study the degree of anisotropy. E1 is the in-plane modulus, E3 refers to the modulus perpendicular to the deposition plane. E1 of sprayed pure steel layers equals 191.4 GPa, which is slightly lower than the moduli of bulk 410 steel (215 GPa) and bulk Eurofer (217 GPa). In contrast, the elastic modulus of sprayed pure W coatings is much lower compared to the modulus of bulk W (229.1 vs. 400 GPa). The moduli of coatings nominally containing 25 (and partially) 50 vol.% W are even lower than the moduli of pure steel layers. This trend was observed in sintered, graded Fe/W composites in [23], too. It is also well-known to occur in cast iron, in which hard graphite precipitates micro-plastically deform the softer matrix upon macroscopically elastic deformation, thus reducing the apparent modulus to lower values than the modulus of the pure matrix [36, 37]. Following this description, in the examined steel-rich coatings, hard constituents (tungsten or intermetallics) may also deform the steel, possibly explaining the trend of Young's modulus with increasing W content. Other aspects influencing the modulus are the amount of pores, cracks and the degree of intersplat bonding. None of these, however, was found exceptionally high or low, respectively, in coatings nominally containing 25 vol.% W.

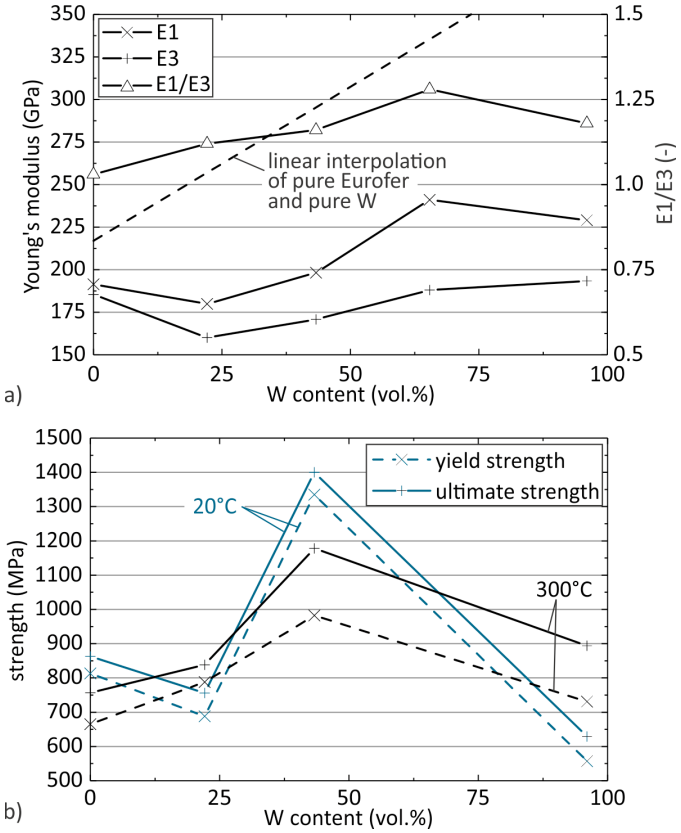

Figure 6: Mechanical properties of uniform coatings, deposited on substrates that were preheated to 700°C. a) Young's modulus, measured at two temperatures and ratio of E1/E3, b) yield strength and ultimate bending strength, measured at two temperatures.

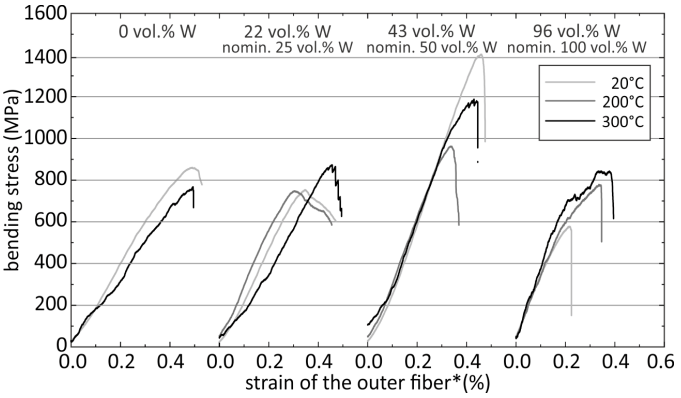

Figure 7: Stress-strain curves obtained from four-point bending tests of uniform coatings, deposited on substrates that were preheated to 700°C. *strain of the outer fiber refers to the position above the notch. Strain after yielding is to be read with care due to the modified testing method, which was only confirmed in the elastic regime.

Comparing E1 and E3, the first exceeds the latter for any layer composition. The ratio E1/E3 is often used as an indicator of the intersplat bonding of sprayed coatings, where isotropic materials yield ratios close to 1. For the present coatings, E1/E3 increases from 1.03 to 1.18 with the W content, indicating a declining intersplat bonding. This result correlates to the observed low thermal conductivity of W-rich layers. Despite the moderate increase of E1/E3, the ratio is close to 1 for all steel/W compositions produced here, suggesting good bonding of adjacent splats compared to literature data [38, 39]. Only coatings nominally containing 75 vol.% W show enhanced anisotropy (E1/E3=1.28) compared to the other coatings.

Regarding strength measurements, samples that were extracted from coatings nominally containing 75 vol.% W fractured instantly when a small load was applied, and were not evaluated. According to fig. 6 b), no monotonous correlation between strength and the W content of the examined layers, and the test temperature, is apparent. Yield strength and ultimate bending strength of steel-rich coatings are high compared to bulk 410 steel, both at room temperature and at 300°C (cf. tab. 3). Quenching and residual stresses from spraying together with fine grains resulting from rapid cooling are assumed to cause the high yield strength. In contrast, W-rich coatings show rather low strength compared to bulk W. This observation correlates to the behaviour of E1/E3 vs. W content, indicating that the layer strength is governed by the intersplat bonding. This result can, however, only partially be confirmed by the morphology of fracture surfaces shown in fig. 8. The surfaces of coatings tested at room temperature document two failure modes: Coatings that contain less than nominally 75 vol.% W locally show smooth areas that correspond to debonded, undeformed splats of pure constituents, steel or W. The failure mode is referred to here as interparticulate failure. In contrast, coatings of $\geq$ 75 vol.% W exhibit more sharp edges. Single, columnar grains with growth in the direction of heat flow during spraying can be observed in the terrace-like structure. This observation indicates transparticulate, intergranular fracture. Fracture surfaces of samples tested at 300°C show the same behaviour. Both failure modes are brittle, which explains the layers' limited capability of hardening after yielding. A correlation of hardening and oxygen content, or porosity is not evident, because even the coatings of lowest oxygen and porosity content exhibit many embrittling defects.

Resulting from the oxides-influenced weak interfaces of steel-rich coatings and the brittle nature of tungsten itself, steel-rich and W-rich coatings fracture at rather low stresses. Coatings nominally containing 50 vol.% W show the highest measured strength. They seem to positively balance the described drawbacks of steel- and W-rich coatings. Moreover, there is likely an improved bonding of unlike splats (i.e. steel+W), as opposed to identical splats (W+W or steel+steel). In case of the latter, new particles typically impact on already solidified material, whereas in case of the former, an incoming W particle (T_m=3400°C) can partially melt the underlying steel (T_m=1500°C), resulting in improved bonding [40]. Coatings of 50 vol.% W contain a high number of dissimilar materials interfaces and benefit from the described effect most.

4. Conclusion

In the present study, pure 410 steel, pure tungsten, uniform steel/W, and graded steel/W layers were produced by water-stabilised atmospheric plasma spraying. The spraying distances

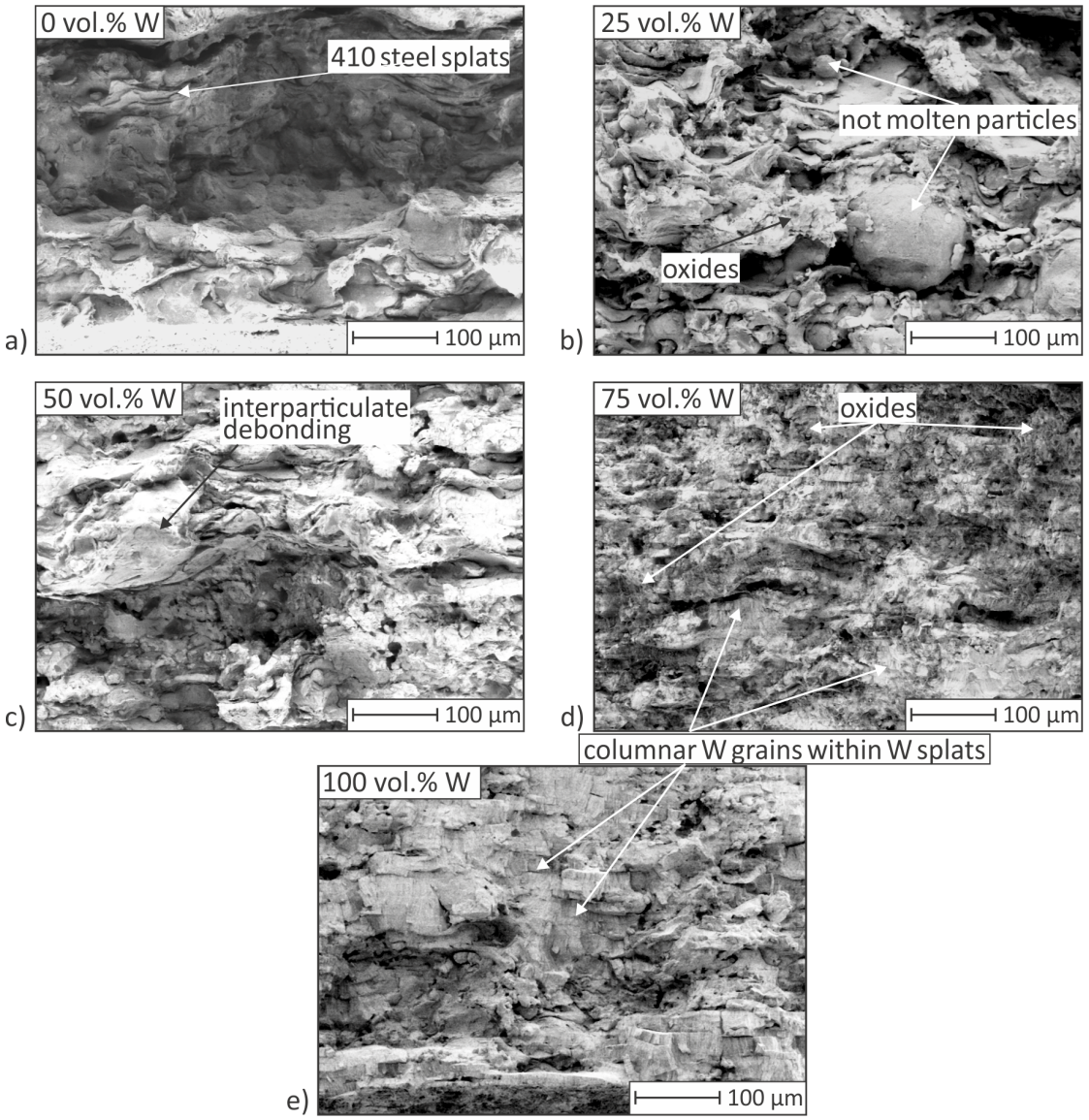

Figure 8: Representative fracture surfaces of coatings, deposited on substrates that were preheated to 700°C, and bent at room temperature. The fracture surface of the nominally 75 vol.% W containing coating oxidised strongly because it was unprotected longer than the other surfaces.

were adjusted according to the volumetric steel/W ratio of the mixed coatings between the ideal spraying distance of pure steel and pure W. A shrouding chamber flushed with a mixture of $Ar+H_2$ was used to limit oxidation of deposited splats, which allowed to preheat the substrates to 900°C in order to improve the density and intersplat bonding.

It was found that uniform mixed coatings and graded coatings exhibit similar microstructures, allowing detailed analyses of the steel/W FGM based on the characterisation of uniform coatings. The porosity of the coatings equals approximately 3 vol.% and is independent from the composition and substrate preheating temperature. The oxide content decreases with increasing W content and is also unaffected by the substrate temperature owing to the shrouding chamber. Compared to plasma spraying without substrate preheating, preheating temperatures of up to 700°C show no negative microstructural developments while potentially increasing the coating cohesion. Beyond 700°C, intermetallic precipitates were found in the coatings, suggesting that 700°C is a favourable preheating temperature. Coatings deposited with this parameter show promising thermo-physical and mechanical properties. Some of these are inferior to properties of Fe/W composites made by FAST or VPS, but when not directly exposed to the plasma, the prepared materials may successfully be implemented in the first wall of fusion reactors. At an early stage of work, the CTE was effectively tailored, which allows to redistribute macro stresses in steel-W joints. The thermal conductivity of all coatings is in the range of Eurofer steel, currently representing the bottle neck of heat removal of the first wall. The conductivity is explained by imperfect intersplat boundaries in the coatings. These were seen in mechanical experiments, too. While the yield strength and ultimate strength of fabricated coatings are superior to Eurofer steel, the brittle-

ness may pose a risk of failure. In order to improve the inter-splat bonding and, consequently, thermal conductivity and ductility, generally, the oxygen contamination is to be reduced and the substrate may be preheated to higher temperatures than used in the present work. The former may be tackled by an improved design of the shrouding chamber, which is currently under way, and by modifying the spraying distance. The latter may occur at the cost of increasing the amount of Fe_xW_y intermetallics in the current material system.

Appendix A. Acknowledgements

This work has been carried out within the framework of the EUROfusion Consortium and has received funding from the Euratom research and training programme 2014-2018 under grant agreement No 633053. The views and opinions expressed herein do not necessarily reflect those of the European Commission. Part of the work was also supported by Czech Science Foundation through grants no. GA17-23154S and no. GA17-13573S.

Appendix B. References

[1] J. W. Coenen, S. Antusch, M. Aumann, W. Biel, J. Du, J. Engels, S. Heuer, A. Houben, T. Hoeschen, B. Jasper, F. Koch, J. Linke, A. Litnovsky, Y. Mao, R. Neu, G. Pintsuk, J. Riesch, M. Rasinski, J. Reiser, M. Rieth, A. Terra, B. Unterberg, T. Weber, T. Wegener, J.-H. You, C. Linsmeier, Materials for DEMO and reactor applications - boundary conditions and new concepts, Physica Scripta T167 (2016) 1–11.

[2] V. Philipps, Tungsten as material for plasma-facing components in fusion devices, Journal of Nuclear Materials 415 (2011) S2–S9.

[3] D. Rapisarda, I. Fernandez, I. Palermo, M. Gonzalez, C. Moreno, A. Ibarra, E. M. de les Valls, Conceptual design of the EU-DEMO Dual Coolant Lithium Lead equatorial module, IEEE Transactions on Plasma Science 44 (9) (2016) 1603–1612.

[4] A. D. Nevo, E. Martelli, P. Agostini, P. Arena, G. Bongiovì, G. Caruso, G. D. Gironimo, P. D. Maio, M. Eboli, R. Giammusso, F. Giannetti, A. Giovinazzi, G. Mariano, F. Moro, R. Mozzillo, A. Tassone, D. Rozzia, A. Tarallo, M. Tarantino, M. Utili, R. Villari, WCLL breeding blanket design and integration for DEMO 2015: status and perspectives, Fusion Engineering and Design 124 (2017) 682–686.

[5] J. Aubert, G. Aiello, J.-C. Jaboulay, B. Kiss, A. Morin, Status on DEMO Helium Cooled Lithium Lead breeding blanket thermo-mechanical analyses, Fusion Engineering and Design 109-111 (2016) 991–995.

[6] S. Heuer, T. Weber, G. Pintsuk, J. Coenen, J. Matějíček, C. Linsmeier, Aiming at understanding thermo-mechanical loads in the first wall of DEMO: Stress–strain evolution in a eurofer-tungsten test component featuring a functionally graded interlayer, Fusion Engineering and Design 135 (2018) 141–153.

[7] ITER Materials Properties Handbook (MPH), ITER Doc. G 74 MA 16 04-05-07 R0.1 (internal project document distributed to the ITER Participants), 2017.

[8] A.-A. F. Tavassoli, A. Alamo, L. Bedel, L. Forest, J.-M. Gentzbittel, J.-W. Rensman, E. Diegele, R. Lindau, M. Schirra, R. Schmitt, H. C. Schneider, C. Petersen, A.-M. Lancha, P. Fernandez, G. Filacchioni, M. F. Maday, K. Mergia, N. Boukos, N. Baluc, P. Spätig, E. Alves, E. Lucon, Materials design data for reduced activation martensitic steel type Eurofer, Journal of Nuclear Materials 329-333 (2004) 257–262.

[9] E. Materna-Morris, C. Adelhelm, S. Baumgärtner, B. Dafferner, P. Graf, S. Heger, U. Jäntsch, R. Lindau, C. Petersen, M. Rieth, R. Ziegler, H. Zimmermann, Structural material Eurofer-2: characterization of rod and plate material: structural, tensile, Charpy and creep properties, Karlsruher Institut für Technologie, 2007.

[10] D. Qu, W. W. Basuki, J. Aktaa, Numerical assessment of functionally graded tungsten/Eurofer coating system for first wall applications, Fusion Engineering and Design 98-99 (2015) 1389–1393.

[11] T. Emmerich, D. Qu, R. Vaßen, J. Aktaa, Development of W-coating with functionally graded W/Eurofer-layers for protection of first-wall materials, Fusion Engineering and Design 128 (2018) 58–67.

[12] M. R. Gilbert, J.-C. Sublet, Handbook of activation, transmutation, and radiation damage properties of the elements simulated using FISPACT-II & TENDL-2015 and Magnetic Fusion Plants, Culham Centre For Fusion Energy, 2016.

[13] P. Gustafson, A thermodynamic evaluation of the C-Fe-W system, Metallurgical Transactions A 18 (1987) 175–188.

[14] W. W. Basuki, J. Aktaa, Process optimization for diffusion bonding of tungsten with Eurofer97 using a vanadium interlayer, Journal of Nuclear Materials 459 (2015) 217–234.

[15] J. Matějíček, B. Nevrlá, M. Vilémová, H. Boldyryeva, Overview of processing technologies for tungsten-steel composites and fgms for fusion applications, Nukleonika 60 (2015) 267–273.

[16] T. Tokunaga, H. Watanabe, N. Yoshida, T. Nagasaka, R. Kasada, Y.-J. Lee, A. Kimura, M. Tokitani, M. Mitsuhara, T. Hinoki, H. Nakashima, S. Masuzaki, T. Takabatake, N. Kuroki, K. Ezato, S. Suzuki, M. Akiba, Development of high-grade VPS-tungsten coatings on F82H reduced activation steel, Journal of Nuclear Materials 442 (2013) S287–S291.

[17] H. Greuner, H. Bolt, B. Böswirth, S. Lindig, W. Kühnlein, T. Huber, K. Sato, S. Suzuki, Vacuum plasma-sprayed tungsten on Eurofer and 316L: Results of characterisation and thermal loading tests, Fusion Engineering and Design 75-79 (2005) 333–338.

[18] Y. Yahiro, M. Mitsuhara, K. Tokunakga, N. Yoshida, T. Hirai, K. Ezato, S. Suzuki, M. Akiba, H. Nakashima, Characterization of thick plasma spray tungsten coating on ferritic/martensitic steel F82H for high heat flux armor, Journal of Nuclear Materials 386-388 (2009) 784–788.

[19] T. Weber, Development and optimization of graded tungsten/eurofer97 joints for divertor components (original title: Entwicklung und Optimierung von gradierten Wolfram/Eurofer97-Verbindungen für Divertorkomponenten), Ph.D. thesis, Karlsruher Institut für Technologie (2012).

[20] Y. Nishi, Y. Mogi, K. Oguri, Preparation of Fe–W amorphous films by an electroplating method, Journal of Materials Science Letters 14 (1995) 1–3.

[21] N. Tsyntsaru, J. Bobanova, X. Ye, H. Cesiulis, A. Dikusar, I. Prosycevas, J. P. Celis, Iron-tungsten alloys electrodeposited under direct current from citrate-ammonia plating baths, Surface and Coatings Technology 203 (2009) 3136–3141.

[22] D. Qu, Z. Zhou, J. Tan, J. Aktaa, Characterization of W/Fe functionally graded materials manufactured by resistance sintering under ultra-high pressure, Fusion Engineering and Design 91 (2015) 21–24.

[23] S. Heuer, T. Lienig, A. Mohr, T. Weber, G. Pintsuk, J. Coenen, F. Gormann, W. Theisen, C. Linsmeier, Ultra-fast sintered functionally graded Fe/W composites for the first wall of future fusion reactors, submitted to Composites Part B: Engineering.

[24] J. Matějíček, M. Vilémová, B. Nevrlá, L. Kocmanová, J. Veverka, M. Halasová, H. Hadraba, The influence of substrate temperature and spraying distance on the properties of plasma sprayed tungsten and steel coatings deposited in a shrouding chamber, Surface & Coating Technology 318 (2017) 217–223.

[25] J. Matějíček, H. Boldyryeva, Processing and temperature-dependent properties of plasma-sprayed tungsten–stainless steel composites, Physica Scripta T138 (2009) 1–4.

[26] P. Sedlak, H. Seiner, J. Zidek, M. Janovska, M. Landa, Determination of all 21 independent elastic coefficients of generally anisotropic solids by resonant ultrasound spectroscopy: Benchmark examples, Experimental Mechanics 54 (2014) 1073–1085.

[27] M. Koller, A. Kruisová, R. Mušálek, J. Matějíček, H. Seiner, M. Landa, On the relation between microstructure and elastic constants of tungsten/steel composites fabricated by spark plasma sintering, Fusion Engineering and Design 133 (2018) 51–58.

[28] S. Antusch, D. E. J. Armstrong, T. B. Britton, L. Commin, J. S. K.-L. Gibson, H. Greuner, J. Hoffmann, W. Knabl, G. Pintsuk, M. Rieth, S. G. Roberts, T. Weingaertner, Mechanical and microstructural investigations of tungsten and doped tungsten materials produced via powder injection molding, Nuclear Materials and Energy 1-2 (2015) 22–31.

[29] ASTM Subcommittee D30.04, Standard Test Method for Flexural Properties of Polymer Matrix Composite Materials (ASTM D7264), ASTM International, 2015.

[30] Deutsche Edelstahlwerke, Material data sheet X12Cr13 1.4006, 2015.
[31] AK Steel Corporation, Material data sheet 410 stainless steel, 2015.
[32] P. L. Fauchais, J. V. R. Heberlein, M. I. Boulos, Thermal Spray Fundamentals - From Powder to Part, Springer, 2014.
[33] J. Matějíček, S. Sampath, D. Gilmore, R. Neiser, In situ measurement of residual stresses and elastic moduli in thermal sprayed coatings Part 2: processing effects on properties of mo coatings, Acta Materialia 51 (2003) 873–885.
[34] J. Matějíček, B. Nevrlá, J. Čech, M. Vilémová, V. Klevarová, P. Haušild, Mechanical and thermal properties of individual phases formed in sintered tungsten-steel composites, Acta Physica Polonica A 128 (2015) 718–721.
[35] R. C. Progelhof, J. L. Throne, R. R. Ruetsch, Method for predicting the thermal conductivity of composite systems: A review, Polymer Engineering and Science 16 (1976) 615 – 625.
[36] D. Lohe, O. Vöhringer, E. Macherauch, The influence of graphite shape on mechanical properties of ferritic cast iron, Mechanical behaviour of materials. Pergamon Press, 1983.
[37] L.-Y. Fang, K. E. Metzloff, R. C. Voigt, C. R. Loper, Der Elastizitätsmodul von graphitischen Gußeisen und Nachdruck des Vortrags "young's modulus in graphitic cast irons." beim 61. Gießerei-Weltkongress, Beijing, ZVG.
[38] M. Vilémová, J. Matějíček, R. Mušálek, J. Nohava, Application of structure-based models of mechanical and thermal properties on plasma sprayed coatings, Journal of Thermal Spray Technology 21 (2012) 372–382.
[39] P. Sedmák, H. Seiner, P. Sedlák, M. Landa, R. Mušálek, J. Matějíček, Application of resonant ultrasound spectroscopy to determine elastic constants of plasma-sprayed coatings with high internal friction, Surface and Coatings Technology 232 (2013) 747–757.
[40] J. Matějíček, M. Vilémová, R. Mušálek, P. Sachr, J. Horník, The influence of interface characteristics on the adhesion/cohesion of plasma sprayed tungsten coatings, Coatings 3 (2013) 108–125.